Robust cross-equalization of 4D-4C PZ migrated data at Teal South

Alexander Druzhinin and Colin MacBeth, Heriot-Watt University*

Summary

A new cross-matching scheme is developed to improve the reliability of time-lapse studies when there are large non-repeatable differences between surveys. Tests on 4D-4C PZ migrated data from the Teal South field, Gulf of Mexico, are used to demonstrate the utility of the approach.

Introduction

The success of seismic monitoring depends largely upon the degree of similarity between 4D data and processing parameters, and is often limited by poor repeatability. This work demonstrates a scheme for producing robust, artefact-free difference volumes from 4D migrated data. Time-lapse repeatability is optimized in regions of no subsurface change by removing non-repeatable seismic acquisition and processing artefacts. The scheme is a modification of that proposed by Rickett and Lumley (1998).

Method

We suggest the following processing workflow:

1. Re-sampling

The first step is the spatial re-sampling of migrated data to a common grid. The B-spline interpolation of instantaneous phase and amplitude obtained from complex-trace analysis (Taner et al., 1979) of the original migrated traces was used to implement this re-sampling. This is necessary as straightforward trace interpolation can impose serious image aliasing problem (e.g., Wolberg, 1994).

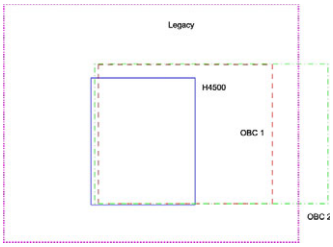

Figure 1. Horizon 4500' sand grid geometry (solid line) and post-stack geometries: legacy (L) survey (dotted line), OBC 1 or B survey (Phase 1, dashed line), and OBC 2 or R survey (Phase 2, dashed and dotted line). The average distance between nearest neighbour traces of the B, R, and L surveys is about 40 ft.

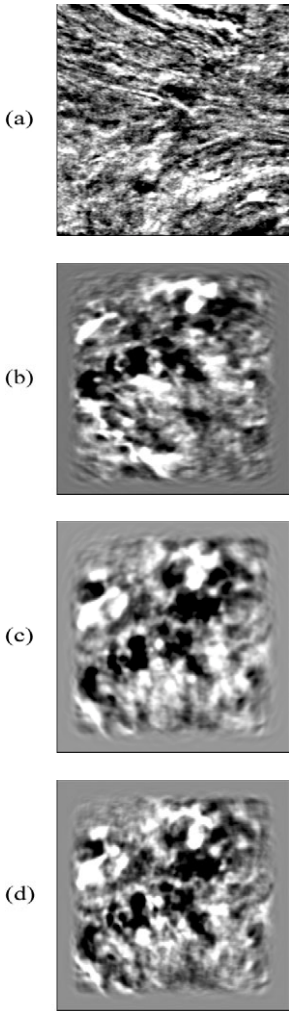

Figure 2. Horizon slice of the 4500' sand from the 4D-4C PZ migrated volumes: (a) L survey, (b) B survey, (c) R survey, and (d) result of cross-matching (M survey).

2. Global cross-equalization

A global matched filter (Grion et al., 2000) is designed over a range of design windows that excludes the reservoir zone. Phase shift and residual statics are estimated from the cross-correlation between traces. This time-domain filter removes severe RMS differences in phase $\bar{\phi}$, reflection strength $\bar{A}$ and time shift $\bar{\tau}$ between the two surveys. An operator was computed from a design window of 500 ms above the reservoir. The legacy dataset was used as the reference.

3. Local spectral balancing

Since repeatability is usually local and frequency dependent, a frequency bandwidth normalization was performed through the use of a generalized cosine window. To ensure that the remaining spectral differences between the surveys were due to production related changes, we selected only frequencies with the best signal-to-noise ratio. The wavelet transform (Deighan and Watts, 1997) is applied to separate signal and noise at this stage.

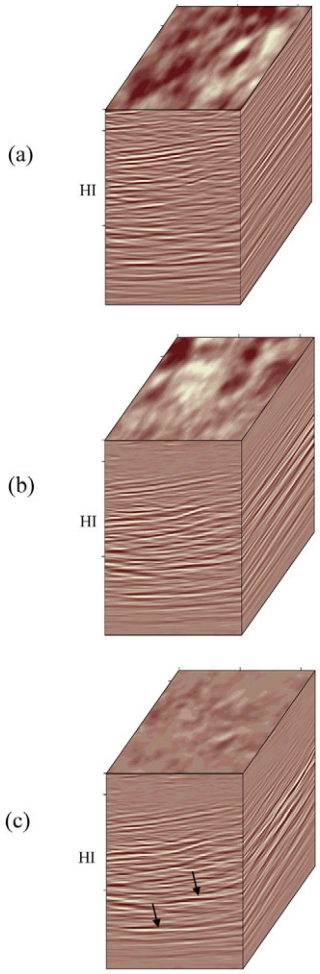

Figure 3. Representative 4D difference volumes below the horizon 4500' sand: (a) global cross-equalization (step 2), (b) geometric warping transformation, and (c) constrained waveform warping transformation (step 4). Arrows indicate possible processing artefacts.

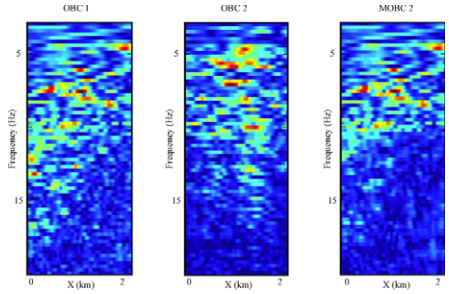

Figure 4. In-line F-X amplitude spectra: OBC 1 survey (left panel) and OBC 2 (middle panel) survey before and after cross-equalization (MOBC 2, right panel).

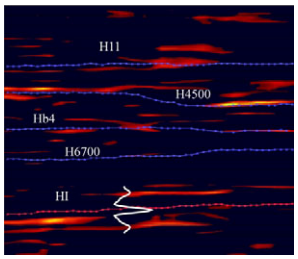

Figure 5. In-line instantaneous amplitude 4D differences and horizon geometries before source deconvolution. Autocorrelation wavelet is shown.

4. Constrained waveform warping transformation

Conventional geometric warping transformations (Wolberg, 1994) provide operators that redefine the spatial relationship between points in an image. Rickett and Lumley (1998) used similar transformations to correct for kinematic differences between surveys. In our approach, the so-called waveform warping transformation incorporates phase-amplitude and geometric warping corrections into a single-pass spatial-temporal filter

$$u = \iint dxdyd\tau\, \bar{A}[w_1 u_1(x,y,t-\bar{\tau})\cos\bar{\phi} - w_2 u_1^H(x,y,t-\bar{\tau})\sin\bar{\phi}], \qquad (1)$$

where u_1 is the reference trace after spectral balancing (step 3) and u_1^H is the Hilbert transform of the trace u_1 (Barnes, 1996). Here, the constraints $\bar{\phi}$, $\bar{A}$, and $\bar{\tau}$ are determined during step 2. The unknown weights w_1 and w_2 are functions of x, y, and τ. Similar to multiple removal schemes (Monk, 1993), they are estimated by matching equation (1) to the filtered second dataset u_2 in the design window. The result is referred to as Constrained Waveform Warping (CWW) transformation. If the local

time shift τ is small, then equation (1) gives a weighted sum of four traces $u_1(t-\bar{\tau})$, $\dot{u}_1(t-\bar{\tau})$, $u_1^H(t-\bar{\tau})$, and $\dot{u}_1^H(t-\bar{\tau})$, where $\dot{u}_1 = \partial u/\partial t$ is the time derivative of u_1 and $\dot{u}_1^H = \partial u^H/\partial t$. The four unknown weights are estimated by matching equation (1) to 100 or more samples of u_2 (see Monk (1993) for details).

5. Complex-trace equalization

It would be very difficult to produce reliable 4D differences directly from the matched (M) and reference data. The difference volume Δu is constructed upon use of the complex-trace analysis of two surveys after cross-equalization. The goal of this analysis is to remove remaining instantaneous phase and amplitude differences everywhere except in the target zone.

6. Calibration step

The ultimate goal of this step is the extraction of the primary reflectivity difference ΔR from the difference volume Δu without making the assumption that the source wavelet is minimum phase. The convolutional model (Robinson and Treitel, 1980) states that

$$\Delta u = \Delta R * f + n, \qquad (2)$$

where f denotes the wavelet (convolution of the source function with the instruments, the geophones, and undesirable effects such as reverberation and ghosting) and n the random noise. A variety of deconvolution techniques provide a stable solution to equation (2) if the wavelet is known (Robinson and Treitel, 1980). The wavelet can be estimated from the equation

$$u = R * f + n, \qquad (3)$$

where u is the output of step 5 and R is the acoustic reflectivity determined from the nearest well. Equation (3) can be solved iteratively. The initial guess can be the autocorrelation wavelet. Sonic log data were averaged to the seismic scale by means of the multi-resolution analysis based upon the wavelet transform (Verhelst and Berkhout, 1997).

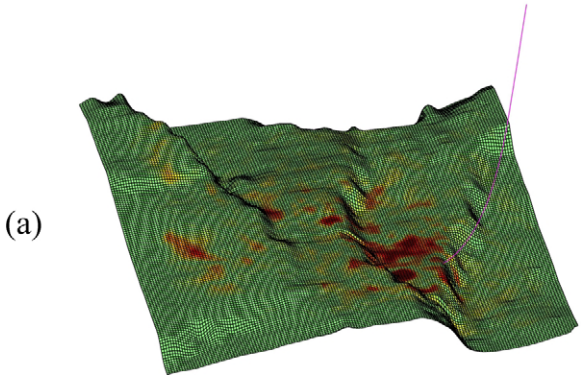

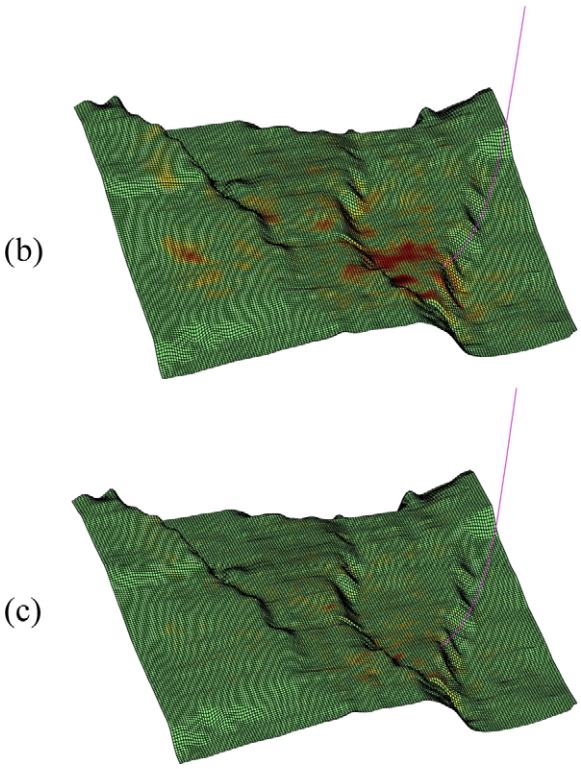

Figure 6. Horizon 4500' sand: 4D reflection strength CWW differences between (a) B and L , (b) R and L, and (c) B and R surveys. Wellpath D10 is shown.

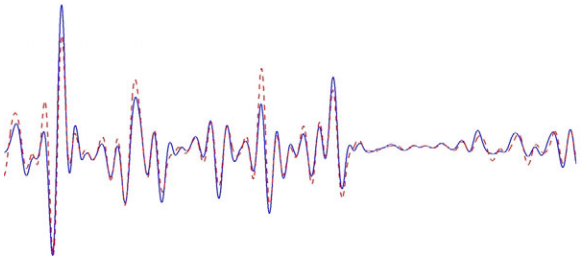

Figure 7. 1-D PP reflectivity for the D11 well after time-frequency upscaling (dashed line) versus PP reflection coefficient estimated from the nearest neighbour trace of the M survey after source deconvolution (solid line). The mean difference between two reflectivity sections is about 23 % of the mean reflection coefficient of 0.24.

Finally, the P-wave impedance change was estimated from the simple formula

$$\Delta\sigma = -\sigma \times \Delta R \times \frac{(1-R)^{-1} + (1+R)^{-1}}{1 + \Delta R/(1+R)} \qquad (4)$$

where $\sigma = AI \times (1-R)/(1+R)$ is the P-wave impedance, AI is the acoustic impedance, and the reflectivity change ΔR is determined from equation (2). In equation (4), it is assumed that the quantities AI and R are compatible with the seismic scale. They were obtained from the averaged sonic log data.

Results from Teal South

Fully migrated 4D-4C PZ images from the Texaco's Teal South field (Ebrom et al., 1998) are used to test the above processing scheme. The purpose of resampling (step 1) is to realign these images onto a common grid representing the horizon 4500' sand (Figure 1). Figure 2 compares the images before and after cross-equalization (step 4). Events in Figures 2c and 2d are directly comparable. The difference amplitudes in Figure 3 become progressively less during the processing steps. By comparing the F-X plots in Figure 4, one can see that spectral differences have also been minimized. Figure 5 shows that the difference amplitudes have their strongest anomalies around the horizons H11, H4500 (4500' sand), Hb4, and HI. Figure 6 is the result of step 5 for the H4500 grid. The sections in Figures 6a and 6b look almost identical due to the relatively low production activity between phases 1 and 2. This is confirmed by the difference section in Figure 6c. Eqs. (2) and (3) were solved to produce a synthetic seismic trace in Figure 7. The impedance change was computed by use of equation (4) (Figure 8). The impedance cross-plot in Figure 9 is very stable. The mean difference is about 3 % of the mean acoustic impedance of 5.47.

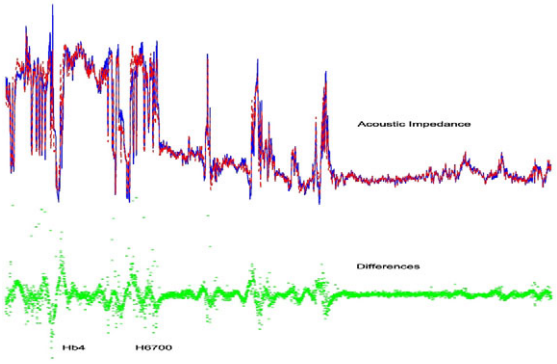

Figure 8. AI (top panel) estimated from PP reflectivity sections in Figure 7: sonic log data (solid line) versus M data (dashed line). Impedance change estimated from equation (4) (bottom panel).

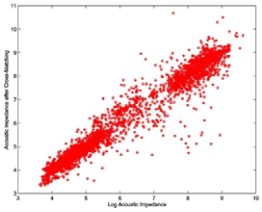

Figure 9. Cross-plot of AI in Figure 8: sonic log data versus M data after step 6.

Conclusions

A new cross-matching scheme has been developed to facilitate time-lapse analysis of migrated 3D volumes with significant non-repeatable differences. Results show that this scheme works well on 4D-4C PZ migrated data from the Teal South field, Gulf of Mexico.

References

Deighan, A. J. and Watts, D. R., 1997, Ground-roll suppression using the wavelet transform, *Geophysics*, **62**,1896-1903.

Ebrom, D., Krail, P., Ridyard, D., and Scott, L., 1998, 4-C/4-D at Teal South. *The Leading Edge*, 17, 1450-1453.

Grion, S., Keggin, J., Ronen, S., and Caldwell, J., 2000, Seismic repeatability benchmarks, *OTC 12099*.

Monk, D.J., 1993, Wave-equation multiple suppression using constrained cross-equalization. *Geophysical Prospecting,* **41**, 725-736.

Rickett, J., and Lumley, D.E., 1998, A cross-equalization processing flow for off-the-shelf 4D seismic data, *SEG Expanded Abstracts*, 16-19.

Robinson, E.A., and Treitel, S., 1980, Geophysical signal analysis, *Prentice-Hall, Inc.*

Taner, M. T., Koehler, F. and Sheriff, R. E., 1979, Complex seismic trace analysis, *Geophysics*, **44**, 1041-1063.

Verhelst, F. and Berkhout, A. J., 1997, Comparison of seismic and borehole data at the same scale, *SEG Expanded Abstracts,* 830-833.

Wolberg, G., 1994, Digital image warping, IEEE Computer Society.

Acknowledgments

The work was supported by the Edinburgh Time-Lapse Project (ETLP) at Heriot-Watt University. The authors would like to thank ERCH Consortium for providing the data and for permission to publish this paper. We are also grateful to Mike Christie, Fiona Reid and Steve Hall (Heriot-Watt University) for their help and useful discussions.